Supplementary Information of Predicting the 3D microstructure of SOFC anodes from 2D SEM images using stochastic microstructure modeling and CNNs

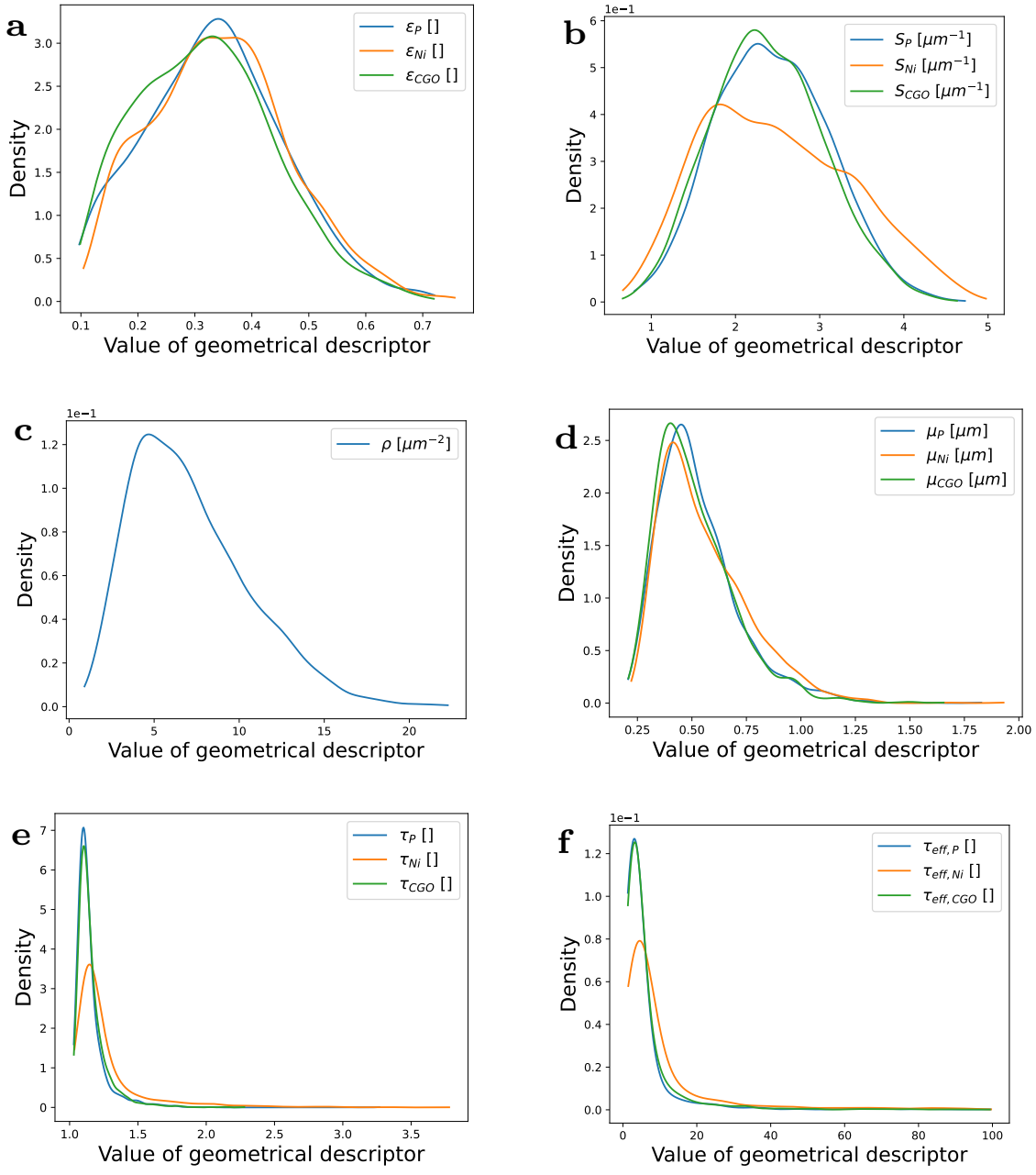

Figure S1. Gaussian kernel density estimators of mean chord lengths (a), specific surface areas (b), specific length of the triple phase boundary (c), volume fractions (d), mean geodesic tortuosities (e) and effective tortuosities (f) based on the 2000 generated ground truth realizations of the stochastic model. For visualization purposes, the plot shows only effective tortuosities with values below 100.

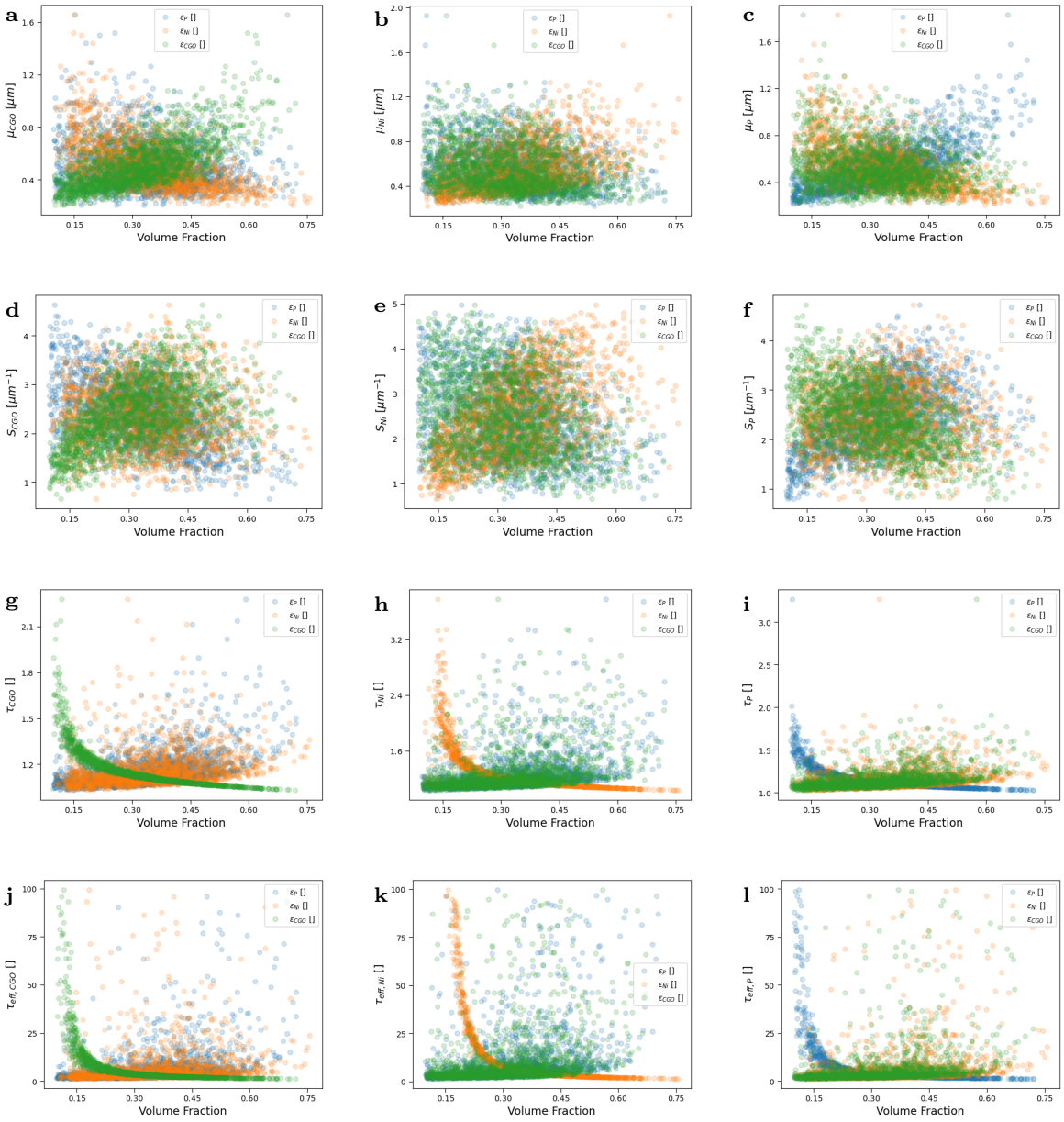

FIGURE S2. Scatter plots, performed on the entire dataset (all 2000 generated ground truth 3D microstructures), showing the relationship between volume fractions of pore (blue), nickel (orange), CGO (green) and the mean chord lengths (a-c), specific surface areas (d-f), mean geodesic tortuosities (g-i) and effective tortuosities (j-l), respectively.

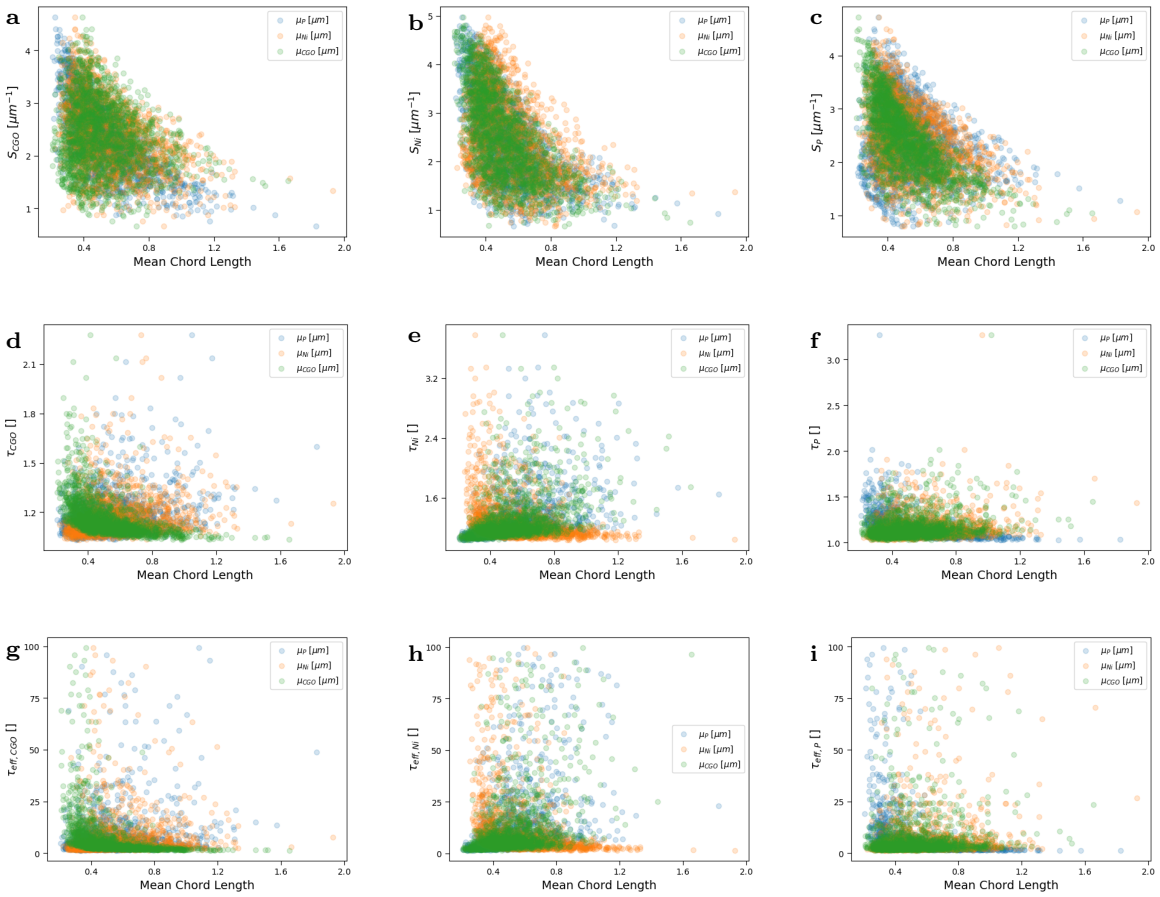

FIGURE S3. Scatter plots, performed on the entire dataset (all 2000 generated ground truth 3D microstructures), showing the relationship between mean chord lengths of pore (blue), nickel (orange), CGO (green) and the specific surface areas (a-c), mean geodesic tortuosities (d-f) and effective tortuosities (g-i), respectively.

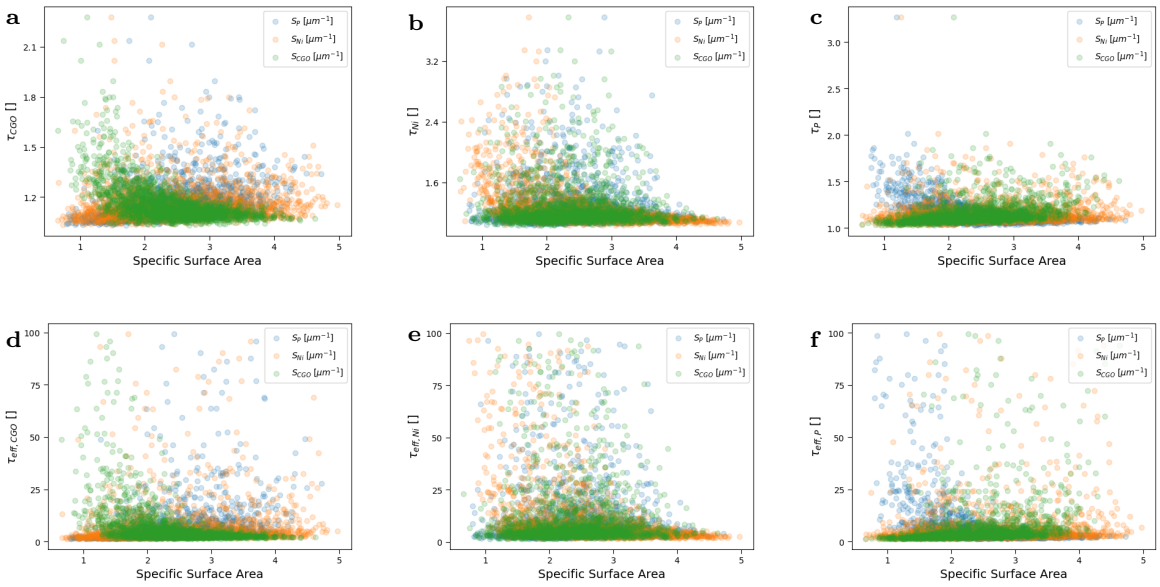

FIGURE S4. Scatter plots, performed on the entire dataset (all 2000 generated ground truth 3D microstructures), showing the relationship between specific surface areas of pore (blue), nickel (orange), CGO (green) and the mean geodesic tortuosities (a-c) and effective tortuosities (d-f), respectively.

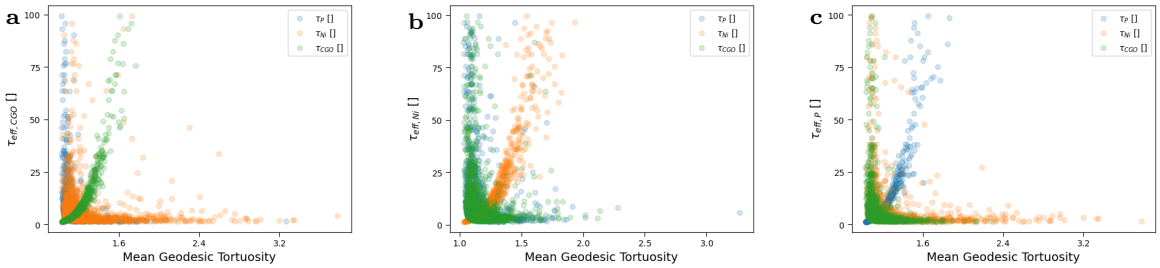

FIGURE S5. Scatter plots, performed on the entire dataset (all 2000 generated ground truth 3D microstructures), showing the relationship between mean geodesic tortuosities of pore (blue), nickel (orange), CGO (green) and the effective tortuosities, respectively.

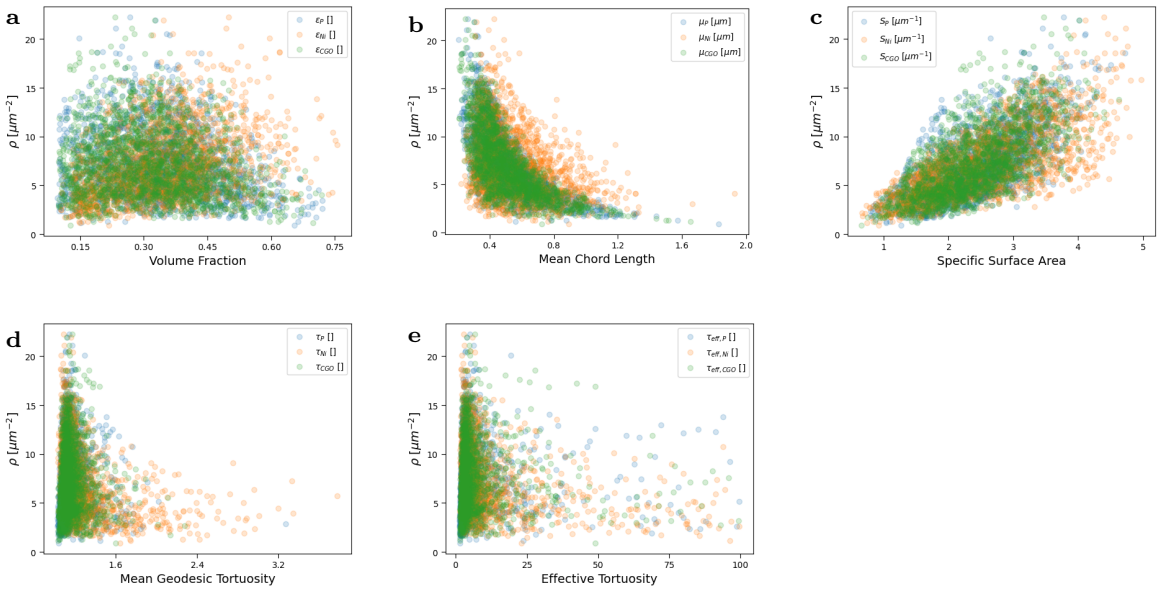

FIGURE S6. Scatter plots, performed on the entire dataset (all 2000 generated 3D microstructures), showing the relationship between the specific length of the TPB and volume fractions (a), mean chord lengths (b), specific surface areas (c), mean geodesic tortuosities (d) and effective tortuosities (e) of pore (blue), nickel (orange) and CGO (green), respectively.

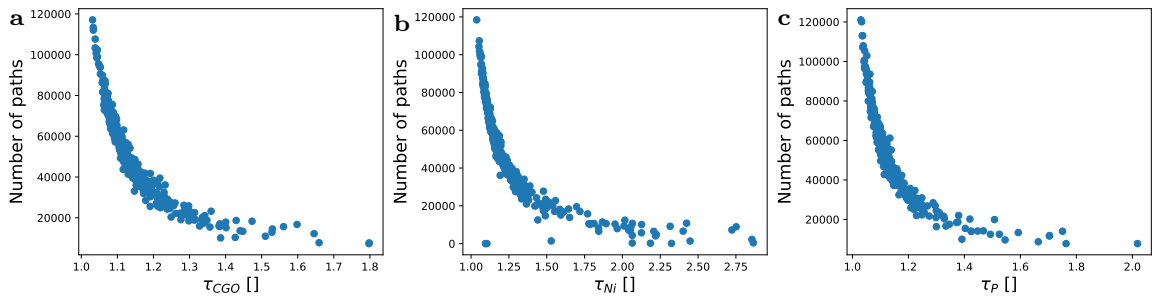

FIGURE S7. Scatter plots, performed on the entire dataset (all 2000 generated ground truth 3D microstructures), showing the relationship between mean geodesic tortuosities and the number of shortest paths from the starting plane to the target plane for CGO (a), nickel (b) and pore (c), respectively.

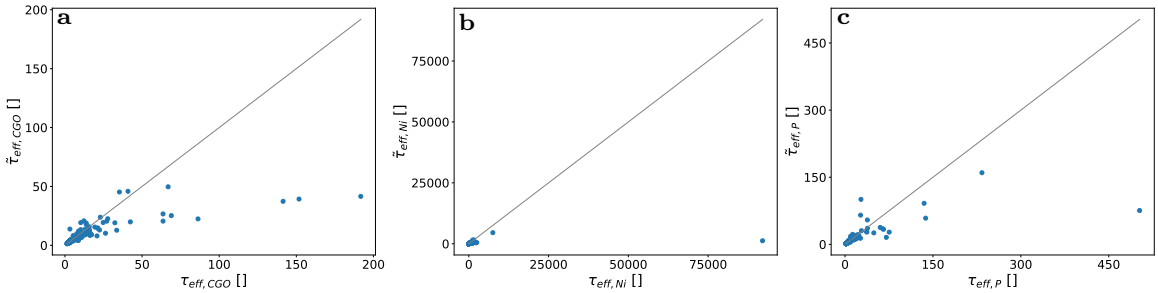

FIGURE S8. Scatter plots showing the relationship between effective tortuosities of ground truth structures on the validation set V and their corresponding predicted structures for CGO (a), nickel (b) and pore (c), respectively.

Descriptor	Front	Middle	Back
$\varepsilon_{\mathrm{CGO}}$ [ ]	0.42	0.43	0.38
$\varepsilon_{\mathrm{Ni}}$ [ ]	0.19	0.22	0.23
ε_{P} [ ]	0.39	0.35	0.39
S_{CGO} [µm^{-1}]	2.14	2.14	2.04
S_{Ni} [µm^{-1}]	0.98	1.03	1.04
S_{P} [µm^{-1}]	2.11	2.03	2.05
μ_{CGO} [µm]	0.74	0.76	0.71
μ_{Ni} [µm]	0.74	0.83	0.84
μ_{P} [µm]	0.70	0.66	0.72
τ_{CGO} [ ]	1.09	1.09	1.10
τ_{Ni} [ ]	1.61	1.46	1.37
τ_{P} [ ]	1.10	1.11	1.10
ρ [µm^{-2}]	2.94	3.09	3.04
$\tau_{\mathrm{eff,\ CGO}}$ [ ]	2.32	2.22	2.59
$\tau_{\mathrm{eff,\ Ni}}$ [ ]	56.8	23.5	18.5
$\tau_{\mathrm{eff,\ P}}$ [ ]	2.57	2.93	2.53

TABLE S1. Comparison of selected geometrical descriptors of the predicted structures. "Front" and "Back" refer to the microstructures reconstructed from the SEM images acquired along the negative and positive z-direction, respectively, while "Middle" denotes the microstructure obtained from an SEM image taken in the negative z-direction with the upper half of the sample removed.